九州工業大学学術機関リポジトリ

Kyutacar

Kyushu Institute of Technology Academic Repository

Photocatalytic reaction over iron hydroxides: A novel visible-light-responsive photocatalyst

Photocatalytic reaction over iron hydroxides: A novel visible-light responsive photocatalyst

Naoya Murakami, Takuma Matsuo, Toshiki Tsubota and Teruhisa Ohno

Department of Applied Chemistry, Faculty of Engineering, Kyushu Institute of Technology, 1-1 Sensuicho, Tobata, Kitakyushu 804-8550, Japan

Abstract

Photocatalytic properties of iron hydroxide (FeOOH) particles prepared by a hydrothermal method were estimated under visible-light irradiation. Hydrothermal treatment in the presence of ethanol induced pure α-FeOOH (goethite) formation even under an acidic condition, while the presence of chloride ion led to preferential formation of β-FeOOH (akaganeite). α-FeOOH particles with largest specific surface area showed the highest photocatalytic activity among commercial and prepared FeOOH samples and exhibited total decomposition of acetaldehyde even under visible-light irradiation. The progress of photocatalytic reaction may be due to multi-electron reduction of oxygen over FeOOH particles.

Keywords: visible-light responsive photocatalyst; iron hydroxide; hydrothermal preparation

* Corresponding author. TEL/FAX: +81-93-884-3318

E-mail address: tohno@che.kyutech.ac.jp (T. Ohno)

1. Introduction

Titanium(IV) oxide (TiO_2) has been a sustainable photocatalyst for environmental remediation because of its nontoxcity, availability, high oxidative potential and chemical stability [1,2]. However, one fault of TiO_2 is that it is inactive in the absence of ultraviolet (UV) light, which hardly exists under indoor illumination condition. Nitrogen-doped TiO_2 is well known as a visible-light-responsive TiO_2 photocatalyst that employs defect absorption attributed to substitutional replacement of Ti or O sites with nitrogen atoms [3,4]. However, its photocatalytic activity under visible light is still low due to defect formation which results in an increase in recombination rate. Recently, tungsten(VI) oxide (WO_3) has attracted much attention as an alternative indoor photocatalyst to conventional nitrogen-doped TiO_2. WO_3 had been believed to be inappropriate for organic decomposition due to inferior reductive potential of the conduction band for one-electron reduction (e.g., $O_2 + e^- = O_2^-$ (aq), -0.284 V vs NHE; $O_2 + H^+ + e^- = HO_2$ (aq), -0.046 V vs NHE), but an efficient decomposition successively proceeds by induction of multi-electron reduction (e.g., $O_2 + 2H^+ + 2e^- = H_2O_2$ (aq), +0.682 V; $O_2 + 4H^+ + 4\ e^- = 2H_2O$, +1.23V) with the aid of a reductive catalyst such as platinum or paradium [5,6]. However, one problem for utilization of WO_3 is high cost due to the uneven distribution of tungsten.

We have reported a visible-light-responsive photocatalyst prepared by hybridization of TiO_2 with trivalent iron (Fe^{3+}) ion, which acts as a sensitizer for a visible light [7]. However, its absorption in the visible-light region of a sample under optimized conditions was still low because of the small amount of modified Fe^{3+} ions. Therefore, larger photoabsorption attributed to band-gap excitation is required for further enhancement of photocatalytic activity. Iron hydroxide (FeOOH) is a low-cost material and a semiconductor absorbing visible light. Although there have been many studies on catalytic, magnetic and gas-sensing properties of FeOOH and iron oxide (Fe_2O_3), photocatalytic properties of FeOOH, especially without additive hydrogen peroxide (H_2O_2), have hardly been reported. In the present study, we evaluated photocatalytic activity for decomposition of acetaldehyde on different kinds of FeOOH, and we investigated the relationship between their properties and activity.

2. Experimental

2.1. Sample preparation

2.1.1. α-FeOOH rod-like particles

Fifty dm^3 of aqueous NaOH solution (2 mol dm^{-3}) was added to 20 dm^3 of aqueous $Fe(NO_3)_3$ solution (20 mmol) with stirring. The solution was transferred into a Teflon bottle, and then the bottle sealed with a stainless jacket was heated at 180 °C for 6 h in an oven. After the hydrothermal treatment, the residue in the Teflon bottle was washed with Milli-Q water several times until ionic conductivity was <10 μS cm^{-1}, and then particles were dried under reduced pressure at 60 °C. This sample is denoted as sample-A1.

2.1.2. α-FeOOH fine particles

Thirty-five dm^3 of ethanol was added to 35 dm^3 of mixed aqueous solution of $Fe(NO_3)_3$ (10 mmol) and $NaNO_3$ (40 mmol). The solution was transferred into a Teflon bottle, and then the bottle sealed with a stainless jacket was heated at 120 °C for 2 h in an oven. After the hydrothermal treatment, the residue in the Teflon bottle was washed with Milli-Q water several times until ionic conductivity was <10 μS cm^{-1}, and then particles were dried under reduced pressure at 60 °C. This sample is denoted as sample-A2.

2.1.3. β-FeOOH needle-like particles

Preparation of β-FeOOH followed the reported method [8]. Thirty five dm^3 of ethanol was added to 35 dm^3 of mixed aqueous solution of $FeCl_3$ (10 mmol) and $NaNO_3$ (70 mmol). The solution was transferred into a Teflon bottle, and then the bottle sealed with a stainless jacket was heated at 120 °C for 2 h in an oven. After the hydrothermal treatment, the residue in the Teflon bottle was washed with Milli-Q water several times until ionic conductivity was <10 μS cm^{-1}, and then particles were dried under reduced pressure at 60 °C. This sample is denoted as sample-B.

2.2. Characterization

Crystal structures of the particles were confirmed by using an X-ray diffractometer (Rigaku, MiniFlex II) with Cu Kα radiation (λ = 1.5405 Å). Diffuse reflectance (DR) spectra were measured using a UV-VIS spectrophotometer (Shimadzu, UV-2500PC) equipped with an integrating sphere unit (Shimadzu, ISR-240A).   The DR spectra were converted to the Kubelka-Munk (K-M) function.   The specific surface areas of the particles were determined with a surface area analyzer (Quantachrome, Nova 4200e) by using the Brunauer-Emmett-Teller equation.   The morphology of prepared TiO_2 particles was observed by using scanning electron microscopy (SEM; JEOL, JSM-6701FONO).

2.3. Photocatalytic decomposition over acetaldehyde

Photocatalytic activities of samples were evaluated by photocatalytic decomposition of acetaldehyde.   One hundred milligrams of powder, which has complete extinction of incident radiation, was spread on a glass dish, and the glass dish was placed in a 125 cm^3 Tedlar bag (AS ONE Co. Ltd.).   Five hundred parts per million of gaseous acetaldehyde was injected into the Tedlar bag, and photoirradiation was performed at room temperature after the acetaldehyde had reached adsorption equilibrium.   The gaseous composition in the Tedlar bag was 79% of N_2, 21% of O_2, < 0.1 ppm of CO_2 and 500 ppm of acetaldehyde, and relative humidity was ca. 30%.   A 500-W xenon lamp (Ushio, SX-UI501XQ) was used as a light source and the wavelength of photoirradiation was controlled by UV-35, L-42 and Y-44 filters (Asahi Techno Glass Co.), and an intensity of 120 mW cm^{-2} was used as the light source.   The concentrations of acetaldehyde and carbon dioxide (CO_2) were estimated by gas chromatography (Shimadzu, GC-8A, FID detector) with a PEG-20 M 20% Celite 545 packed glass column and by gas chromatography (Shimadzu, GC-9A, FID detector) with a TCP 20% Uniport R packed column and a methanizer (GL Sciences, MT-221), respectively.

3. Results and discussion

3.1. Crystal structures of prepared samples

Figure 1 shows XRD patterns of commercial and prepared samples. Commercial FeOOH (Nacalai Tesque) and sample-A1 have only α-FeOOH (goethite) without other crystal phases. Sample-A2 also has an α-FeOOH structure, but peaks with low intensity and broad peak width were observed in the pattern, indicating that sample-A2 was fine particles. Moreover, a small peak at ca. 24.1 degrees attributed to α-Fe_2O_3 (hematite) structure was observed, though the content was only a few percent.

Preparation procedures for α-FeOOH have been reported by many groups, but most of them were prepared under basic conditions because acidic conditions without structure control additives induced formation of Fe_2O_3. In the present study, low-temperature hydrothermal synthesis with additive ethanol induced α-FeOOH formation even under an acidic condition. An increase in ethanol content has been reported to slow hydrosis of Fe^{3+} as a result of pH decrease [8]. Therefore, α-FeOOH was mainly formed due to retardation of crystal transformation to α-Fe_2O_3. Actually, α-Fe_2O_3 appeared by the hydrothermal process under a high temperature and/or longer hydrothermal duration even in the presence of ethanol.

Figure 1b indicates that sample-B consists of a β-FeOOH (akaganeite) structure without other crystal phases. Cl^- ion from $FeCl_3$ as a starting material is thought to lead to the formation of β-FeOOH because the detailed molecular structure of the β-FeOOH can be expressed as $FeO(OH)_{1-x}Cl_x$ [8].

Primary particle size along the hkl direction (D_{hkl}) was estimated using the Scherrer equation ($D_{hkl} = 0.9\lambda/\beta_{hkl}\cos\theta_{hkl}$, where λ is the wavelength of X-rays, β_{hkl} is the full width at half maximum and θ_{hkl} is the Bragg angle attributed to the hkl plane). The values of D_{110} were 29 nm, 27 nm, 22 nm and 13 nm for commercial FeOOH, sample-A1, sample-A2 and sample-B, respectively.

3.2. Photoabsorption properties of prepared samples

Figure 2 shows DR spectra converted to the Kubelka-Munk function of commercial and prepared samples. The spectra showed visible-light absorption, and the absorption edge appeared around

550-600 nm. These results agree with reported band-gap values of α-FeOOH and β-FeOOH, which are 2.0-2.5 eV and 2.12 eV, respectively [9,10]. A large difference in the absorption edge between α-FeOOH and β-FeOOH was not observed, and sample-A2 showed an appreciable red shift compared to other samples. Considering the absorption edge of α-Fe_2O_3 (Fig. 3e), the existence of α-Fe_2O_3, a trace amount of which was contained in sample-A2, may contribute to the red shift of its absorption edge.

3.3.   Observation of surface structures of prepared samples

Figure 3 shows SEM images of commercial and prepared FeOOH samples. Commercial FeOOH and sample-A1 had a similar rod-like structure, but sample-A1 was smaller particles with well-defined exposed crystal faces attributable to the {110} face compared with the commercial sample [11]. Sample-A2 was fine particles of 50-100 nm in diameter. Primary particle size estimated using the Scherrer equation (22 nm) indicates that the particles observed by SEM were secondary particles formed as a result of aggregation of fine primary particles.   Sample-B particles were also aggregated, and showed a needle-like shape with longer and shorter diameters of ca. 100 nm and ca. 20 nm, respectively.

3.4.   Photocatalytic activity for acetaldehyde decomposition

Photocatalytic activity was evaluated by decomposition of acetaldehyde. Figure 4 shows the time course of CO_2 evolution for acetaldehyde decomposition under photoirradiation, the wavelength of which was longer than ca. 350 nm. Photocatalytic reaction increased with an increase in specific surface area (18 m^2 g^{-1} for commercial FeOOH, 25 m^2 g^{-1} for sample-A1, 138 m^2 g^{-1} for sample-A2 and 116 m^2 g^{-1} for sample-B), and a linear relationship between activity and specific surface area was observed, indicating that specific surface area is the main factor for photocatalytic activity of FeOOH.   In contrast, commercial and prepared α-Fe_2O_3 which was obtained by calcination of sample-A2 at 250 ^{o}C for 2 h, showed only slight photocatalytic activity under the same conditions.

Another plausible reason for the high photocatalytic activity of sample-A2 is the mixture of crystal phase of α-FeOOH and α-Fe_2O_3, which may induce a synergetic effect, e.g., charge separation through interface charge transfer or Z-scheme reaction [12]. In order to confirm this, a physical mixture sample of sample-A1 and α-Fe_2O_3 prepared by calcination of sample-A2 at 250 ^{o}C for 2 h was prepared in the ratio of 9:1. However, an increase in photocatalytic activity was not observed by the physical mixture. This result indicates that sample-A2 showed the highest photocatalytic activity due to its large specific surface area.

Photocatalytic activity of sample-A2, which exhibited the highest activity among the prepared samples, was evaluated under visible-light irradiation (Fig. 4b). Photocatalytic activity was decreased under photoirradiation with a longer wavelength, but visible-light activity was clearly observed. Total decomposition of acetaldehyde, i.e., 1000 ppm of CO_2 evolution, was observed even under visible-light irradiation, but it took a longer photoirradiation time (ca. 60 h under photoirradiation with a Y-44 filter). Flat band potential of α-FeOOH is reported to be 0.32 V (pH 6.5) [9,13]. This may imply reduction of oxygen over FeOOH was induced by not one-electron reduction but multi-electron reduction. Higher photocatalytic activity of smaller FeOOH particles is a reasonable result since multi-electron reduction proceeds more easily on small particles than on larger ones [14]. H_2O_2 produced by the multi-electron reduction possibly contributes to subsequent oxidation reaction by hydroxyl radical (OH·) production, which is induced by photo-fenton reaction between Fe^{2+} and H_2O_2. The reason for less activity of α-Fe_2O_3 may be its inferior oxidation potential of the valence band and/or its less hydration surface state, which may be related to production of H_2O_2.

4. Conclusion

Photocatalytic activity of FeOOH with different particle sizes and crystal structures was investigated under UV-visible and visible-light irradiation. Photocatalytic activity of FeOOH samples increased with an increase in specific surface area, and 1000 ppm evolution of CO_2 was observed over sample-A2 even under visible-light irradiation. These results suggest multi-electron

reduction of oxygen takes place over FeOOH particles because conduction band potential of FeOOH is reported to be less negative than one-electron reduction potential of oxygen.

References

[1] A. Fujishima, T. N. Rao, D. A. Tryk, J. Photochem. Photobiol. C: Photochem. Reviews 1 (2000) 1.

[2] M. R. Hoffmann, S. T. Martin, W. Choi and D. W. Bahnemann, Chem. Rev. 95 (1995) 69.

[3] S. Sato, Chem. Phys. Lett. 123 (1986) 126.

[4] R. Asahi, T. Morikawa, T. Ohwaki, K. Aoki, Y. Taga, Science 293 (2001) 269.

[5] R. Abe, H. Takami, N. Murakami, B. Ohtani, J. Am. Chem. Soc., 130 (2008) 7780.

[6] T. Arai, M. Horiguchi, M. Yanagida, T. Gunji, H. Sugihara, K. Sayama, Chem. Commun., 2008, 5565.

[7] N. Murakami, T. Chiyoya, T. Tsubota, T. Ohno, Appl. Catal. A: Gen. 348 (2008) 148.

[8] H. Shao, X. Qian, J. Yin, Z. Zhu, J. Solid State Chem. 178 (2005) 3130.

[9] D.M. Sherman, Geochim. Cosmochim. Acta, 69 (2005) 3249.

[10] A.F. White, Rev. Mineral. 23 (1990) 467.

[11] P. Ou, G. Xu, Z. Ren, X. Hou, G. Han, Mater. Lett. 62 (2008) 914.

[12] T. Arai, M. Yanagida, Y. Konishi, Y. Iwasaki, H. Sugihara, K. Sayama, J. Phys. Chem. C, 111 (2007) 7574.

[13] W. Du, Y. Xu, Y. Wang, Langmuir 24 (2008) 175.

[14] T. Hirakawa, Y. Nakaoka, J. Nishino, Y. Nosaka, J. Phys. Chem. B 103 (1999) 4399.

Figure captions

Figure 1.   (A) XRD patterns of (a) ICDD PDF-2 data (No. 01-081-0464), (b) commercial FeOOH, (c) sample-A1 and (d) sample-A2.   (B) XRD patterns of (a) ICDD PDF-2 data (No. 00-034-1266) and (b) sample-B.

Figure 2.   Diffuse reflectance spectra converted to the K-M function of (a) commercial FeOOH, (b) sample-A1, (c) sample-A2, (d) sample-B and (e) commercial α-Fe$_2$O$_3$.

Figure 3.   SEM images of (a) commercial FeOOH, (b) sample-A1, (c) sample-A2 and (d) sample-B.

Figure 4.   (A) Time courses of CO_2 evolution of acetaldehyde decomposition over (a) commercial FeOOH, (b) sample-A1, (c) sample-A2 and (d) sample-B under photoirradiation with a UV-35 filter. (B) Time courses of CO_2 evolution of acetaldehyde decomposition over sample-A2 under photoirradiation with (a) UV-35, (b) L-42 and (c) Y-44 filters.

Figure1A
Click here to download high resolution image
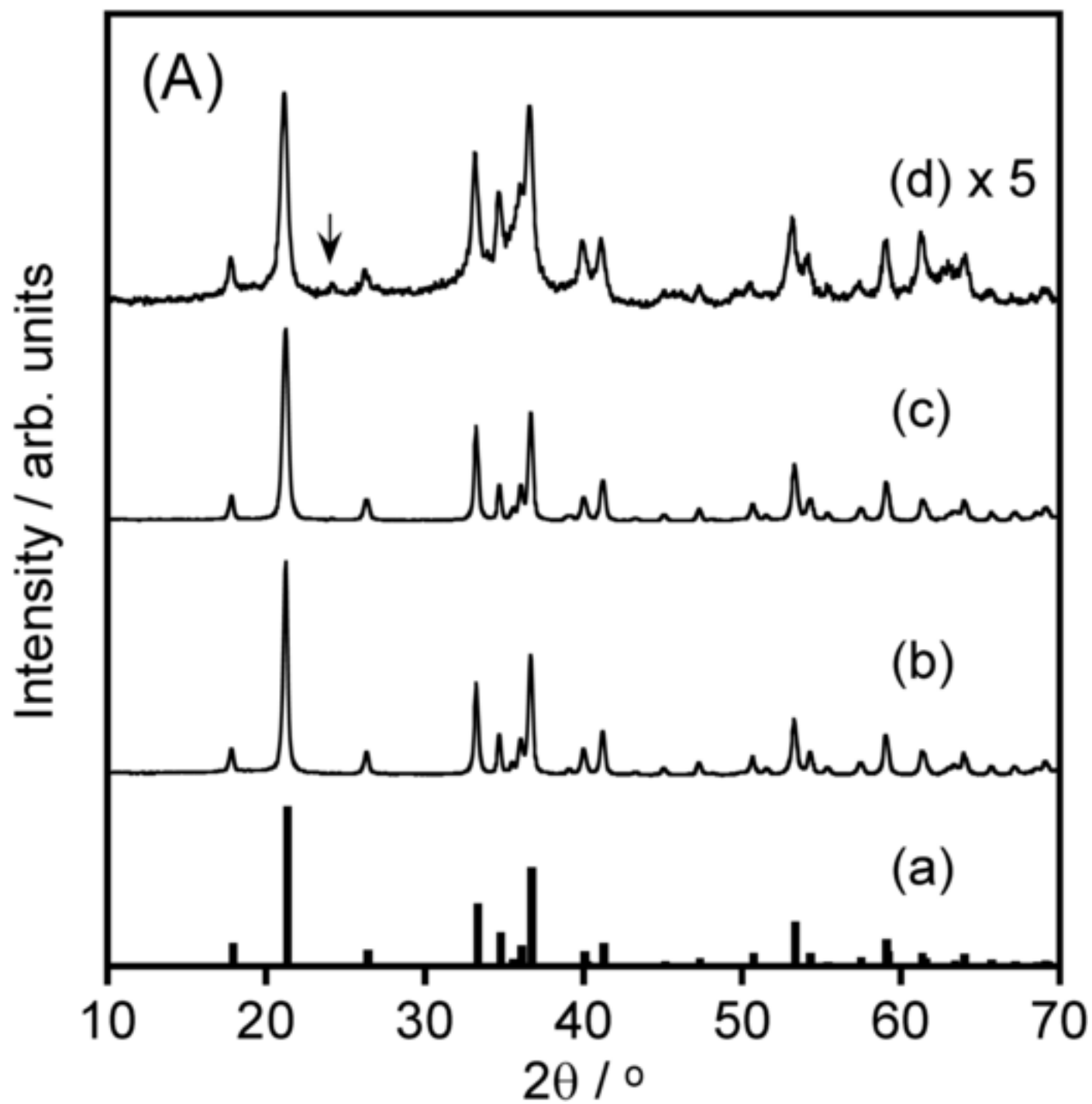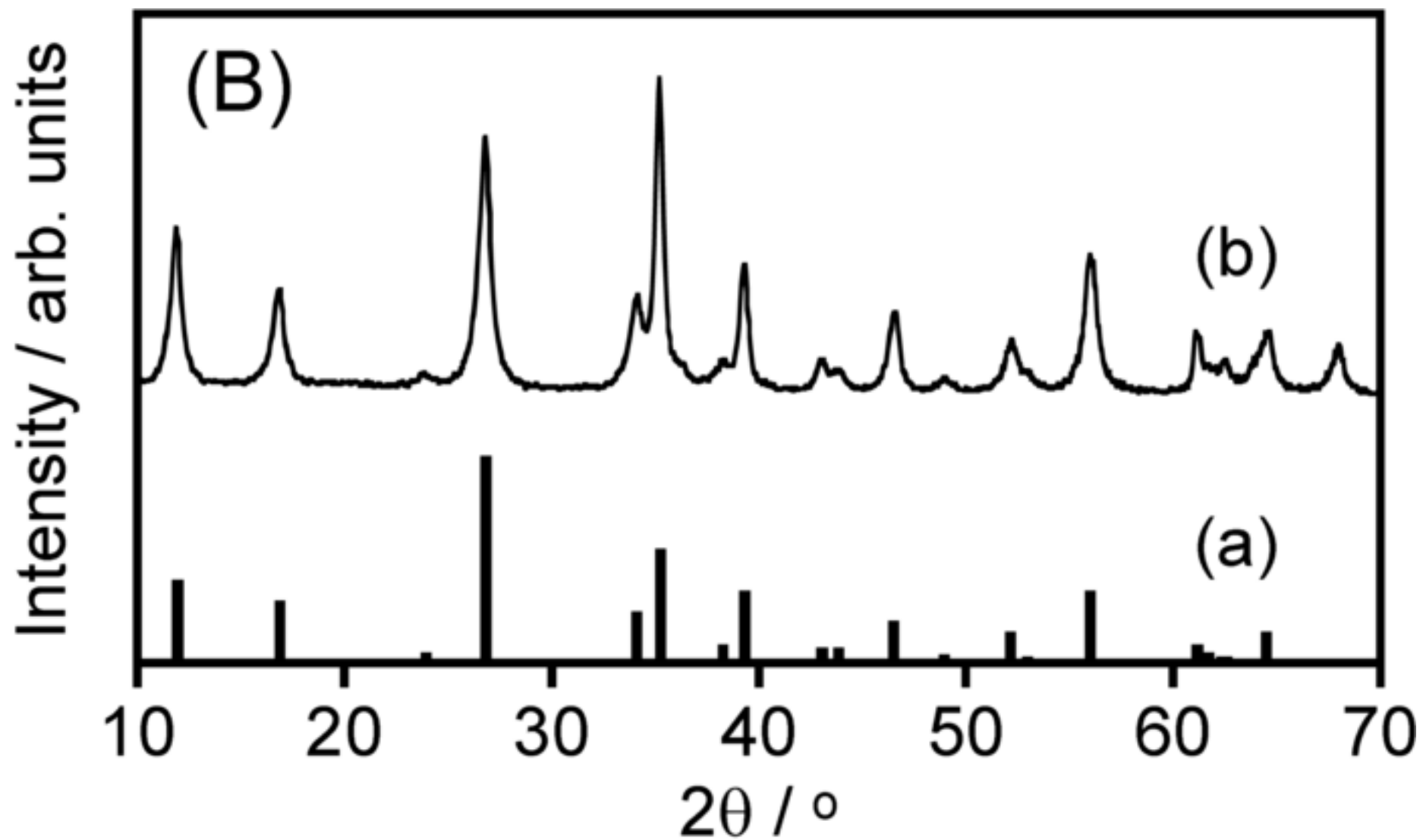
Figure2
Click here to download high resolution image

Figure3
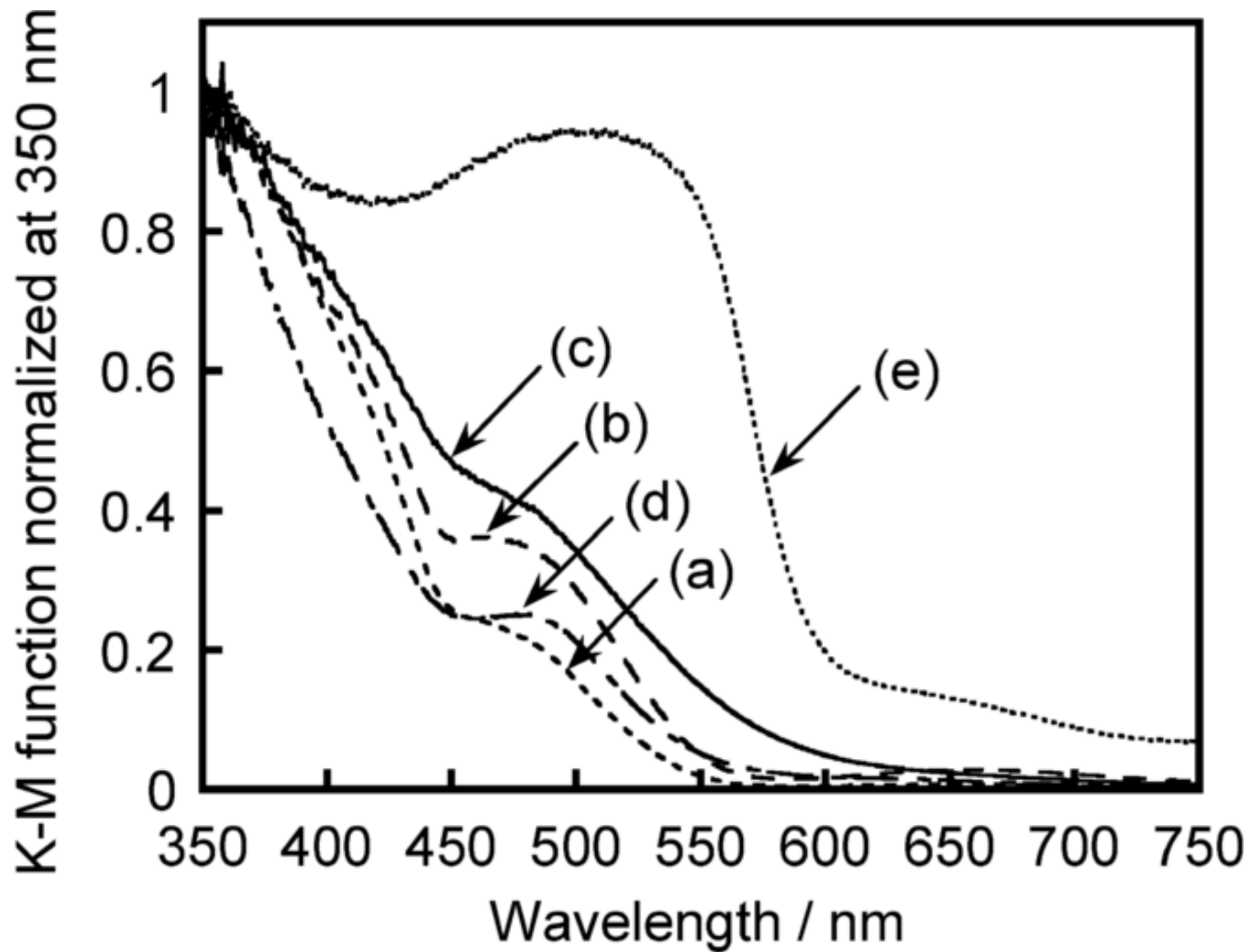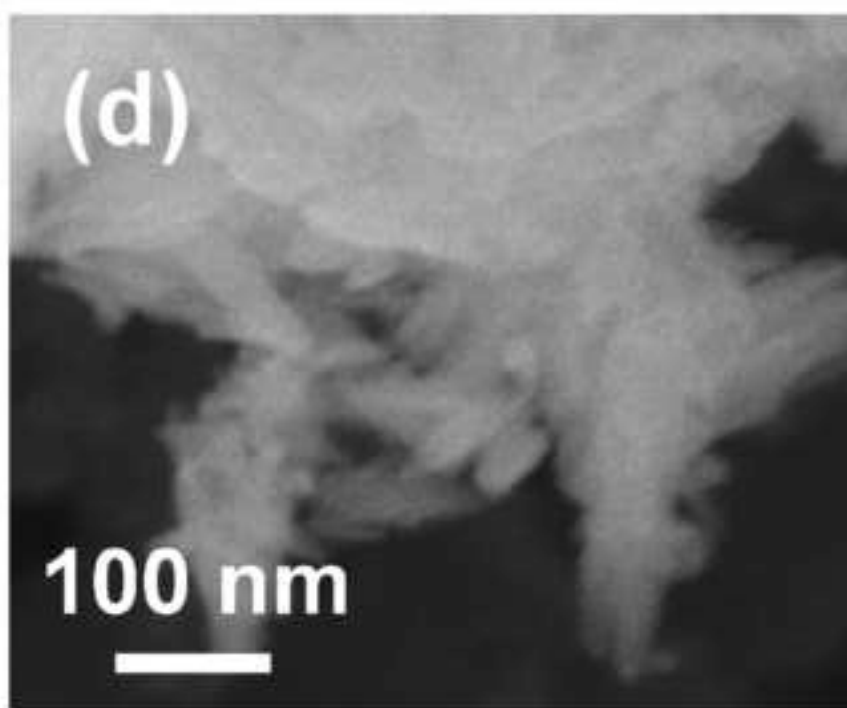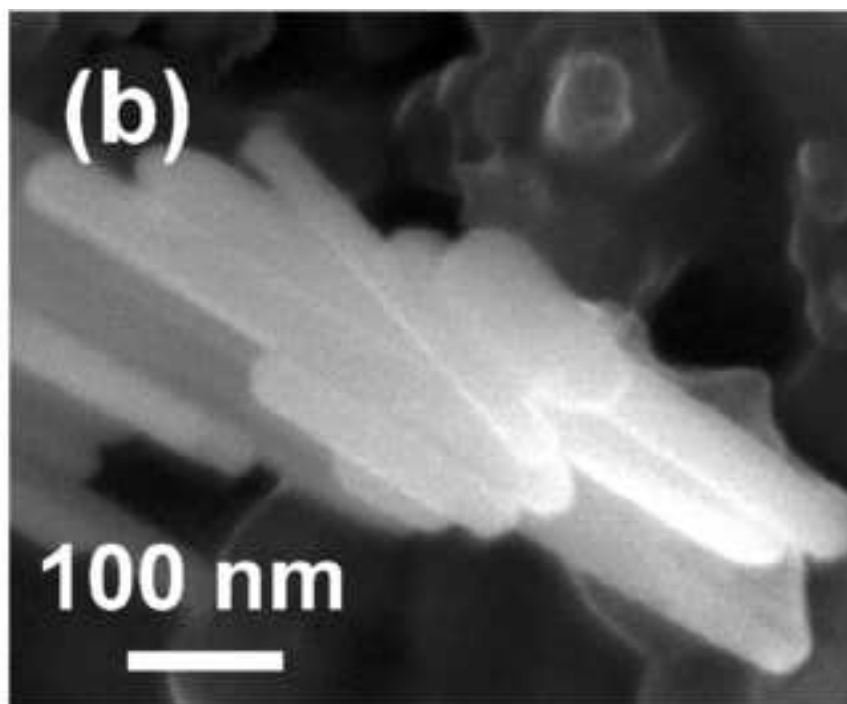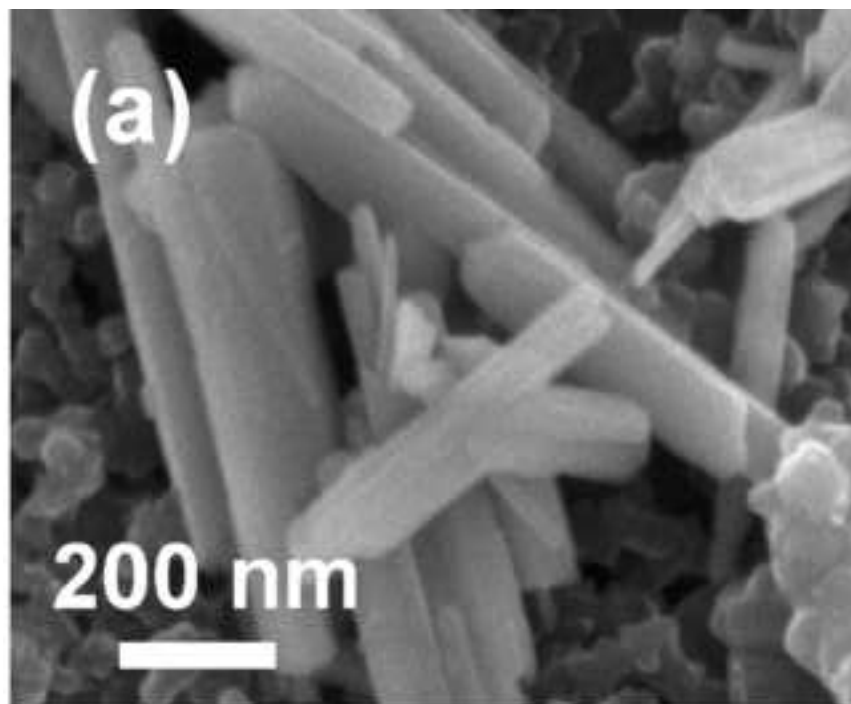**Click here to download high resolution image**

Figure4